inorganics

MDPI

Article

Synthesis, Crystal Structure, and Luminescent Sensing Properties of a Supramolecular 3D Zinc(II) Metal–Organic Framework with Terephthalate and Bis(imidazol-1-yl)methane Linkers

Vladislava V. Matveevskaya, Dmitry I. Pavlov, Alexey A. Ryadun, Vladimir P. Fedin * and Andrei S. Potapov *

Nikolaev Institute of Inorganic Chemistry, 3 Lavrentiev Ave., 630090 Novosibirsk, Russia; matveevskaya@niic.nsc.ru (V.V.M.); pavlov@niic.nsc.ru (D.I.P.); ryadunalexey@mail.ru (A.A.R.)
* Correspondence: cluster@niic.nsc.ru (V.P.F.); potapov@niic.nsc.ru (A.S.P.); Tel.: +7-383-330-92-56 (A.S.P.)

Abstract: Supramolecular 3D Zn(II) coordination polymer {[Zn(bim)(bdc)]·0.8DMF·0.4EtOH·0.1H_2O}$_n$ (**Zn-MOF**), constructed from Zn^{2+} ions, bis(imidazol-1-yl)methane (bim) and terephthalate (bdc^{2-}) anions, was synthesized and structurally characterized. **Zn-MOF** crystallizes in the tetragonal crystal system, space group $P4_2/n$. Each Zn(II) ion coordinates two neutral bim molecules in a bridging bidentate coordination mode via nitrogen atoms at position 3 of the imidazole rings and two bdc^{2-} anions, with monodentate coordination of the carboxylate group for one of them and bidentate coordination for another. Zn(II) cations are in a distorted square pyramidal ZnN_2O_3 coordination environment. Metal cations are alternately linked by the bim and bdc^{2-} ligands, forming a two-dimensional layered structure along the crystallographic plane *ab*. As a result of layer interpenetration, a supramolecular 3D network is formed. **Zn-MOF** demonstrated blue (aquamarine) emission with a maximum at 430 nm upon excitation at 325 nm. The luminescence lifetime of 6 ns is characteristic for ligand-centered fluorescence. The luminescent sensing properties of **Zn-MOF** in ethanol suspension toward inorganic cations and anions were evaluated and an emission quenching response was observed for Fe^{3+} and chromate/dichromate ions. Photoinduced electron transfer from **Zn-MOF** to Fe^{3+} was elucidated as a possible quenching mechanism on the basis of DFT calculations.

Keywords: zinc; metal–organic framework; bis(imidazol-1-yl)methane; terephthalic acid; crystal structure; luminescence; sensing

Citation: Matveevskaya, V.V.; Pavlov, D.I.; Ryadun, A.A.; Fedin, V.P.; Potapov, A.S. Synthesis, Crystal Structure, and Luminescent Sensing Properties of a Supramolecular 3D Zinc(II) Metal–Organic Framework with Terephthalate and Bis(imidazol-1-yl)methane Linkers. *Inorganics* **2023**, *11*, 264. https://doi.org/10.3390/inorganics11070264

Academic Editors: George Gamov and Elena Antina

Received: 25 May 2023
Revised: 20 June 2023
Accepted: 21 June 2023
Published: 22 June 2023

1. Introduction

The development of society in the direction of raising living standards requires increased attention to environmental monitoring and minimizing the negative impact of environmental threats on human health. Over the past few decades, the release of hazardous chemicals into the environment from industrial and other anthropogenic processes has caused severe global environmental problems. Chemicals such as heavy metal ions, toxic inorganic anions, volatile organic compounds, etc. [1–3] are non-degradable and pose a persistent threat to human health. These pollutants can enter and accumulate in living organisms, including humans, causing a range of health problems such as cancer [4], neurological disorders [5], and reproductive issues [6]. Therefore, monitoring environmental pollutants is paramount to reducing contamination risks. However, detecting trace pollutants remains a significant challenge in the field of environmental protection. Despite the many analytical methods currently used for identifying environmental pollutants, fluorescence-based detection has distinct advantages, including high sensitivity, selectivity, and ease of manipulation and visualization. As such, it represents an ideal alternative for detecting pollutants.

Fe^{3+} ions have become increasingly important in biological and environmental systems due to their crucial role in the cellular metabolism, synthesis of DNA and RNA, and oxygen uptake processes [7]. A moderate concentration of Fe^{3+} ions is necessary to maintain the normal metabolism in living systems, while an excess or deficiency of Fe^{3+} leads to the development of various pathological conditions such as hepatic cirrhosis, endotoxemia, and hereditary hemochromatosis. Since Fe^{3+} excess may result from excessive absorption from the environment, the development of methods for the selective detection of Fe^{3+} ions is an urgent and important undertaking. As of today, several techniques have been used to detect and quantify Fe^{3+} in solution: spectrophotometry, voltammetry, inductively coupled plasma mass spectrometry (ICP-MS), and atomic absorption spectrometry. Among these methods, fluorescent detection offers a simplistic approach with high sensitivity, accuracy, and economy for online monitoring and detection of Fe^{3+} ions, making it a favorable choice. However, the widespread use of fluorescent sensors is currently limited by their cross-sensitivity to other metal ions such as Cu^{2+}, Cr^{3+}, Al^{3+}, and Pb^{2+} [8–15].

Chromium is extensively used in various industrial applications such as alloy production, pigments, paints and dyes, chrome plating, and corrosion control. However, excessive intake of Cr(VI) anions, such as $Cr_2O_7^{2-}$ and CrO_4^{2-}, can be severely cytotoxic and carcinogenic, causing significant disruptions to the DNA, protein, and enzyme systems of the human body. Therefore, the efficient sensing of $Cr_2O_7^{2-}$ and CrO_4^{2-} anions is of utmost importance. However, compared to metal ions and nitroaromatic explosives and other pollutants, sensors for the detecting of $Cr_2O_7^{2-}$ and CrO_4^{2-} anions remain relatively limited.

To overcome this limitation, there has been significant progress in the development of luminescent metal–organic frameworks (MOFs) for detecting various ions over the past few years [16–20]. Metal–organic frameworks (MOFs), also known as porous coordination polymers, are a novel type of crystalline porous material composed of inorganic metal ions or clusters and suitable ligands. The MOFs' permanent porosity can enhance the sensitivity of the analytes by potentially preconcentrating them. Additionally, the porosity provides an ideal environment to accommodate substrates and induce differential recognition through intermolecular interactions between the framework and the analytes, making them highly promising as chemical sensors. However, despite the significant progress made in the application of luminescent MOFs for the sensing of guest species, only a few luminescent MOF-based sensors are capable of quantitative detection. Furthermore, the MOF-based sensors' sensitivity, stability, and especially their recyclability need improvement. The properties of luminescent MOFs can be precisely engineered by selecting ligands and metals with desired characteristics. The widespread mixed-ligand approach was used in this work, since the combination of carboxylate ligands with aromatic π-system on the one hand and N,N-donor bitopic linkers on the other can afford novel luminescent MOFs. Among the transition metal ions with d^{10} electron configuration, Zn^{2+} is commonly used for the synthesis of MOFs due to its excellent coordination ability and low cost, as well as its lower toxicity compared to Cd^{2+} ions, which are also commonly used for luminescent MOF synthesis. 1,4-Benzenedicarboxylic (terephthalic) acid (H_2bdc) represents a rigid linker forming strong metal–oxygen coordination bonds, while neutral N,N-donor ligand, bis(imidazole-1-yl)-methane (bim) is an efficient bitopic bridging linker joining the MOF building units into 2D or 3D nets [21–24].

So far, Zn-based MOFs constructed from bis(imidazolyl)methane and dicarboxylate ligands are rather limited. Interestingly, Yang and Bu recently successfully assembled bim ligand and various carboxylic acids such as 1,3,5-benzenetricarboxylic acid and 4,4′-oxybis(benzoic acid with Zn(II) to form 1D zigzag chain and 2D coordination polymers. Thermal stability and photoluminescent properties were studied and briefly discussed [25]. Chen and coworkers reported a Zn(II) coordination polymer prepared from bim ligand and iminodiacetate, which demonstrate high thermal stability and strong blue emission [26]. Synthesis and characterization of 1D coordination polymer prepared from bim ligand and 1,3,5-benzenetricarboxylic acid was reported by Qin and coworkers [27]. The authors note

that the polymer shows remarkable photoluminescent properties. Li reported synthesis and structural characterization of Zn(II) coordination polymer based on bim ligand and 5-hydroxylisophthalate acid. The coordination polymer exhibits 1D tube-like structure, with D_{2h}-symmetric cyclic $(H_2O)_4$ tetramer encapsulated in the 1D tubes [28]. Xu and coworkers investigated the coordinating behavior of bim ligand towards Zn(II) ions in the presence of various carboxylic acids such as 2,2′-bipyridine-3,3′-dicarboxylic acid, 2-chloronicotinic acid, adipic acid, malonic acid, and citric acid. In total, five new coordination compounds were reported. The coordination polymers exhibited different 3D topologies due to different coordination modes of carboxylates and bim ligand functionality [29]. Very recently, Ghoshal et al. reported two Zn-complexes built by employing dim and fumarate ligands. They demonstrated single crystal to single crystal transformation for one of the complexes by selective elimination of lattice methanol. Textural properties of the frameworks were studied as well, and it was found that the polycatenated framework surprisingly is more efficient at hydrogen adsorption [30].

According to abovementioned considerations, Zn^{2+} was assembled with the π-conjugated organic ligand H_2bdc and bim to obtain a supramolecular 3D coordination polymer, $\{[Zn(bim)(bdc)]\cdot 0.8DMF\cdot 0.4EtOH\cdot 0.1H_2O\}_n$ (**Zn-MOF**, Scheme 1), which was structurally characterized. The luminescent characteristics of **Zn-MOF** demonstrate its potential use as a turn-off luminescent probe for detecting Fe^{3+} and $Cr_2O_7^{2-}$ ions.

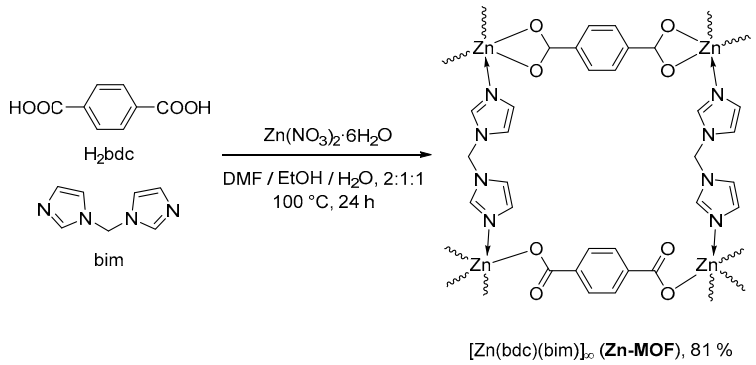

Scheme 1. Synthesis of **Zn-MOF**.

2. Results and Discussion

2.1. Synthesis and Characterization of **Zn-MOF**

The interaction between zinc(II) nitrate $Zn(NO_3)_2\cdot 6H_2O$, terephthalic acid, and bis(imidazol-1-yl)methane in DMF-EtOH-H_2O (2:1:1) mixture at 100 °C for 24 h lead to the formation of single crystals of $\{[Zn(bim)(bdc)]\cdot 0.8DMF\cdot 0.4EtOH\cdot 0.1H_2O\}_n$ (**Zn-MOF**, Scheme 1). Its crystal structure was determined by single-crystal X-ray diffraction (SCXRD) and the phase purity of the bulk product was confirmed by powder X-ray diffraction (Figure 1).

According to the thermogravimetric analysis, the removal of solvate DMF, EtOH, and H_2O molecules starts at 260 °C and ends at 310 °C (Figure S1, the observed weight loss 17.0%, calculated for 0.8DMF + 0.4EtOH + 0.1H_2O 17.2%). The composition of the solvate molecules (43 electrons, 145 Å^3 per formula unit) is in accordance with the number of electrons removed from the cavities in the structure (36 electrons, 136 Å^3 per formula unit) by PLATON SQUEEZE routine [31]. The results of the elemental (CHN) analysis confirm the chemical composition of **Zn-MOF** and correspond to the SCXRD data and thermogravimetric data. The loss of solvate molecules at such high temperature may be explained by the positioning of the solvate molecules in closed cavities according to the SCXRD analysis (see Section 2.2). The desolvated **Zn-MOF** is stale up to about 340 °C and a quick decomposition takes place above this temperature (Figure S1). The IR spectrum of **Zn-MOF** (Figure S2) contains a medium intensity and broad absorption band in the 3560–3327 cm^{-1} region which can be attributed to the presence of water and ethanol

solvate. The strong and broad bands at 1676 and 1600 as well as at 1392 and 1352 cm^{-1} are ascribed to the asymmetric and symmetric stretching vibrations of the bridging and chelating carboxylate groups of the BDC^{2-} ligand, respectively. Separations between the asymmetric and symmetric stretching frequencies $\Delta\nu$ are 284 and 248 cm^{-1}, which is in agreement with bidentate and monodentate coordination modes for the carboxylate groups [32].

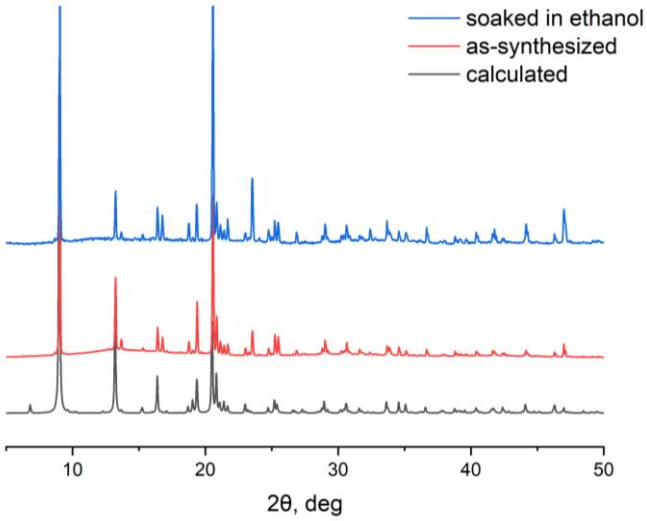

Figure 1. PXRD pattens of as-synthesized **Zn-MOF** and after soaking in ethanol.

2.2. Crystal Structure of **Zn-MOF**

According to the single crystal XRD analysis, **Zn-MOF** crystallizes in the tetragonal crystal system, space group $P4_2/n$. The asymmetric unit of **Zn-MOF** includes one Zn^{2+} ion with one coordinated bim ligand and one terephthalate dianion (Figure 2a). The coordination environment of each Zn^{2+} ion is distorted square pyramidal, the structural parameter τ_5 is 0.36 (should be 0 for ideal square pyramidal and 1 for trigonal bipyramidal) [33]. The apical positions are occupied by N(1) atoms of the imidazole rings in one of the bridging bim ligands, with the distance Zn–N(1) = 2.025 Å which is typical for Zn(II) coordination compounds of bim ligand [34,35]. The four basal coordination sites are occupied by N(2) atoms of the imidazole rings in the second bridging bim ligand (Zn–N = 2.041 Å) and three oxygen atoms of the terephthalate anions with a monodentate coordination of the carboxylate group for one of them (distance Zn-O(3) = 1.943 Å) and bidentate coordination for another (distances Zn-O(1) and Zn-O(2) = 1.987 and 2.547 Å, respectively). The adjacent Zn^{2+} ions are interconnected by the terephthalate bdc^{2-} anions to produce an infinite zinc–carboxylate zig-zag chain along the crystallographic axis *b* (Figure 2b). The two-dimensional folded layer structure is composed of Zn^{2+} ions from the adjacent chains connected by bim ligands along the axis *a* (Figure 2c). It should be noted that one of the bim positions is disordered, as it happens to be located at one of the inversion centers. As follows, there are two positions related by the inversion operation with an occupancy of 0.5 (Figure S3).

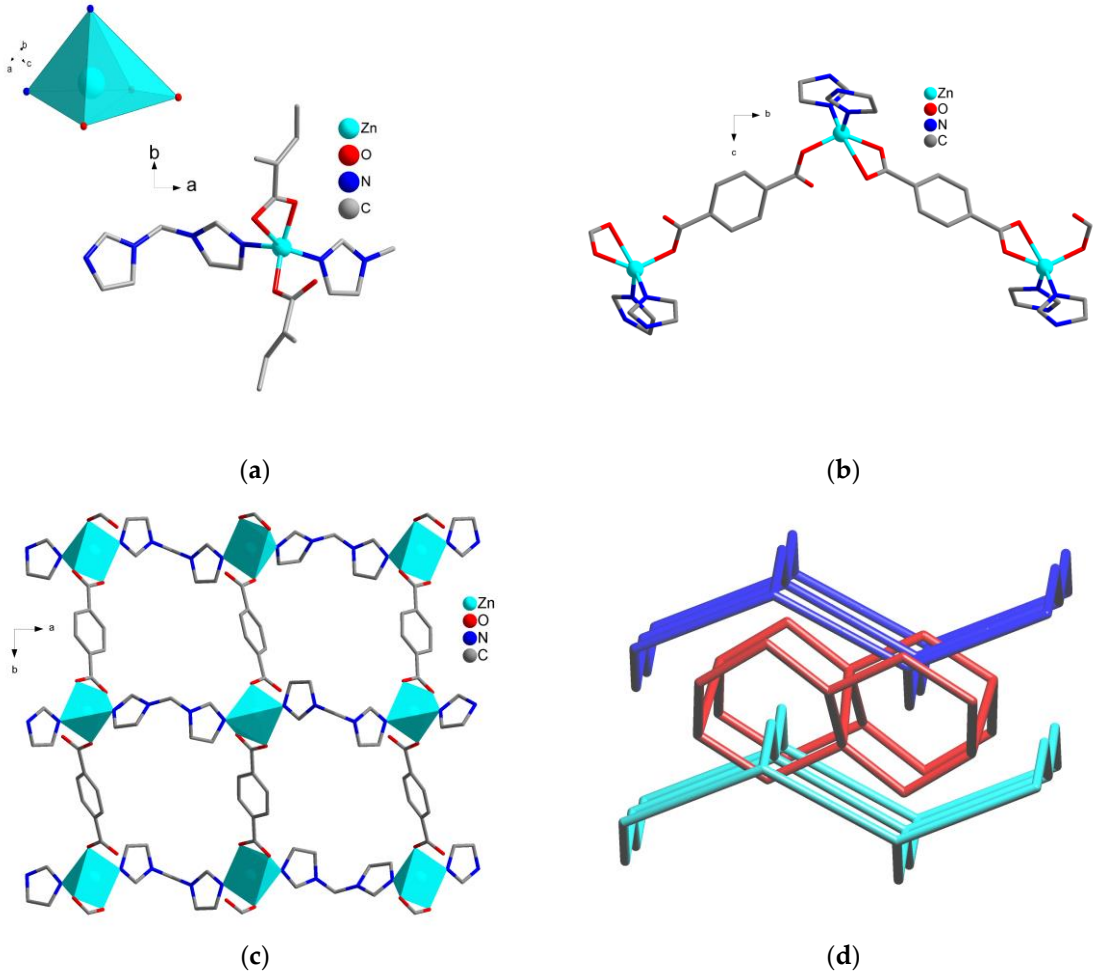

Figure 2. Crystal structure of **Zn-MOF**: (**a**) Asymmetric unit of **Zn-MOF**; (**b**) Zinc–carboxylate chain propagating along the crystallographic axis *b*; (**c**) Structure of 2D layer; (**d**) Topological representation of the layer polycatenation.

The topological representation of **Zn-MOF** structure was generated with the aid of ToposPro software [36]. In a topological sense, the layer of **Zn-MOF** may be represented as 4-connected uninodal sql net with point symbol $4^4.6^2$; however, because of 2D + 2D polycatenation (angled bim fragments of the separate layers cross each other), a 3D supramolecular framework is formed. As can be seen from the net representation of **Zn-MOF** layer packing, they are woven together by the bim units. Each layer is rotated 90 degrees relative to the previous one (Figure 2d). Polycatenation of the layers results in the formation of closed voids in the structure of **Zn-MOF** with the free volume of 29% of the unit cell (Figure S4).

Hirshfeld surface analysis of intermolecular interactions in **Zn-MOF** crystal structure (Figure 3) and calculation of 2D fingerprint plots (Figure S4) were carried out using the CrystalExplorer program [37]. Hirshfeld surface analysis is a rapidly emerging technique that enables a comprehensive understanding of the intermolecular interactions within a crystal structure using a fingerprint plot. This technique offers an easy identification of characteristic interactions throughout the structure or as a surface around the molecule. For **Zn-MOF**, the major contribution to intermolecular interactions (57.7%) is provided by C···C interactions, while C···O and C···N interactions provide partial contributions of 16.8% and 5.9%, respectively (Figure S5).

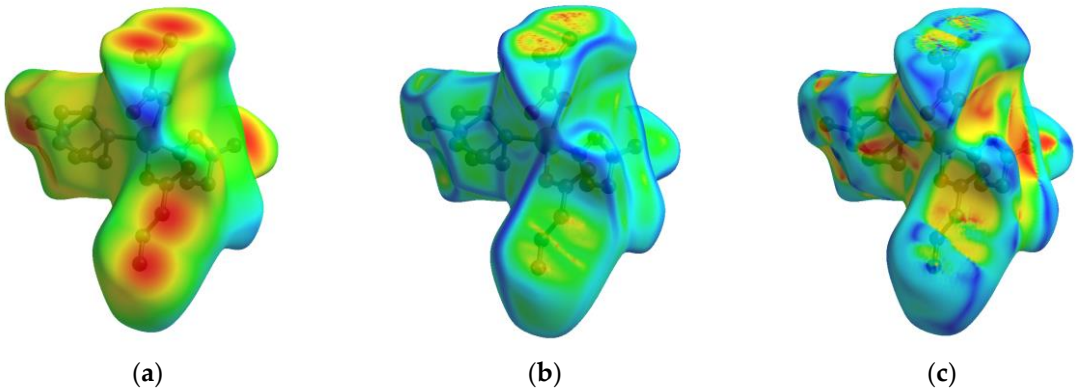

(**a**) (**b**) (**c**)

Figure 3. Hirshfeld surfaces for **Zn-MOF** mapped with: (**a**) d_e; (**b**) Curvedness; (**c**) Shape index.

2.3. Luminescent Properties

The luminescent properties of **Zn-MOF** and the ligands bim and H_2bdc were studied in the solid state at room temperature. H_2bdc ligand exhibited emission with the maximum near 385 nm upon excitation at 290 nm (Figure S6). It is interesting to note that the bim ligand exhibited excitation-dependent emission. When the bim ligand is excited with the two excitation peaks (300 nm and 320 nm), the corresponding emission spectra demonstrate maxima at 327 nm and 383 nm with a large difference of 56 nm (Figure S7a). When the excitation is varied from 280 nm to 350 nm, the emission peak of bim undergoes a red shift as large as 84 nm (Figure S6b). Previously, similar photophysical behavior was observed for 1,3-bis(2-methylimidazol-1-yl)propane [38,39]. The emission spectrum of **Zn-MOF** was independent of the excitation wavelength and exhibited a bathochromic shift of the emission band with the maximum near 430 nm (Figure 4a). The CIE1971color coordinates determined from the emission spectrum of **Zn-MOF** (0.1728, 0.2921) correspond to aquamarine color (Figure 4b).

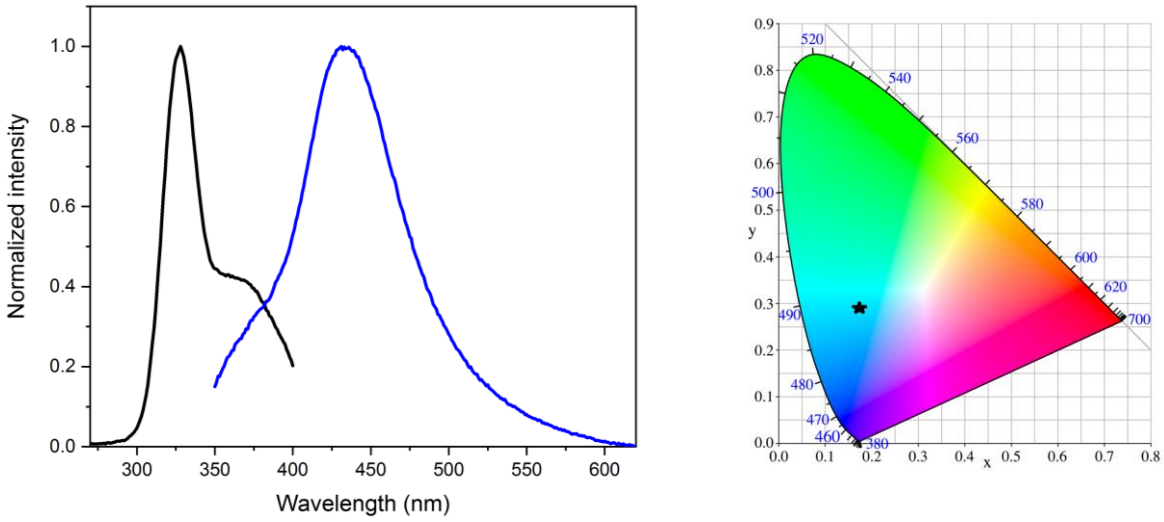

(**a**) (**b**)

Figure 4. Luminescent properties of **Zn-MOF**: (**a**) Excitation (black line, λ_{em} = 430 nm) and emission (blue line, λ_{ex} = 325 nm) spectra; (**b**) CIE-1931 chromaticity diagram, the star indicates the emission color.

The luminescence decay kinetics of **Zn-MOF** at room temperature can be described by the biexponential dependence $I = A_1 \cdot \exp(-t/\tau_1) + A2 \cdot \exp(-t/\tau_2) + A_0$ (Figure S8). The calculated luminescence lifetimes τ_1 and τ_2 are 1.7 and 6.2 ns (relative amplitudes are

1% and 99%, respectively). The observed luminescence lifetimes are characteristic for ligand-centered fluorescence.

2.4. Luminescent Sensing of Inorganic Anions and Cations

Zn-MOF was tested as a luminescent probe of detecting various ions. The stability of **Zn-MOF** powder in ethanol was confirmed by PXRD analysis (Figure 1). In addition, to confirm the stability of the Zn-MOF suspension in ethanol, luminescence spectra were recorded at intervals of 1–2 min for 15 min. It was noted that the intensity of the emission did not change significantly in the specified time interval, which is enough to carry out the analytical determination (Figure S9). A stable suspension of **Zn-MOF** in ethanol was prepared and its emission response to inorganic anions and metal cations was evaluated. Aqueous solutions of different inorganic anions (sodium salts, I^-, Br^-, Cl^-, SCN^-, SO_4^{2-}, NO_3^-, CrO_4^{2-}, $Cr_2O_7^{2-}$, $1{\cdot}10^{-2}$ M) and metal cations (nitrates, Cd^{2+}, Mg^{2+}, K^+, Pb^{2+}, La^{3+}, Ga^{3+}, Al^{3+}, Cu^{2+}, Hg^{2+}, Fe^{3+}, $1{\cdot}10^{-2}$ M) were added to the ethanol suspension of **Zn-MOF**. The luminescence spectrum of the resulting suspension was obtained under the same conditions. As shown in Figure 5 and Figure S10, only the samples containing Fe^{3+} and $Cr_2O_7^{2-}$ displayed a significant quenching effect on the emission intensity of **Zn-MOF**, which indicates that it may serve as a potential luminescent turn-off sensor for Fe^{3+} and $Cr_2O_7^{2-}$ ions.

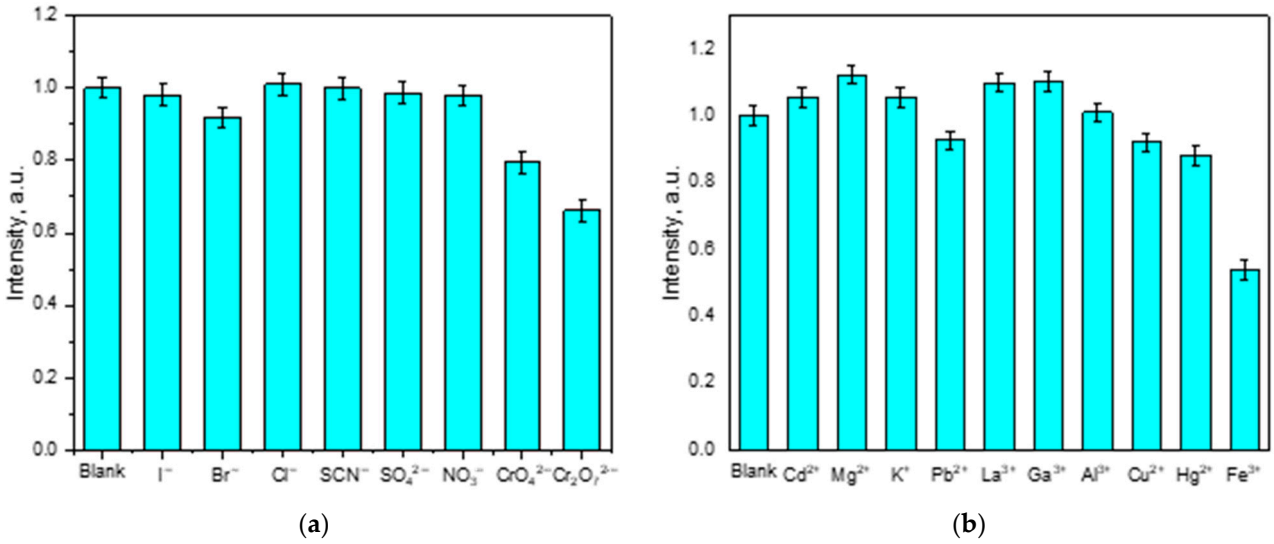

(**a**) (**b**)

Figure 5. Integral emission intensities (from 400 nm to 640 nm) of **Zn-MOF** ethanol suspensions upon excitation at 330 nm in the presence of $1{\cdot}10^{-4}$ M of: (**a**) Inorganic anions; (**b**) Metal cations.

Possible reasons for **Zn-MOF** luminescence quenching were evaluated using DFT calculations. For this purpose, the energies of frontier molecular orbitals of **Zn-MOF** were calculated. To make calculations feasible, a model of MOF structure was used, resembling one zinc cation, two coordinated bim ligands, and two coordinated bdc^{2-} ligands. The excessive negative charge was compensated for by two lithium cations coordinated to the carboxylate groups that are not bound to zinc (Figure S11a). Previously, we used this approach to model the metal centers in MOFs [40,41]. The quenching agent was modeled as a hexaaquairon(III) cation, $[Fe(H_2O)_6]^{3+}$ (Figure S11b).

The highest occupied molecular orbital (HOMO) of **Zn-MOF** is localized on the imidazole ring of bim ligand (Figure 6a), while the lowest unoccupied molecular orbital (LUMO) is localized solely on bdc^{2-} ligand (Figure 6b); thus, the excitation process may be described as a ligand-to-ligand charge transfer.

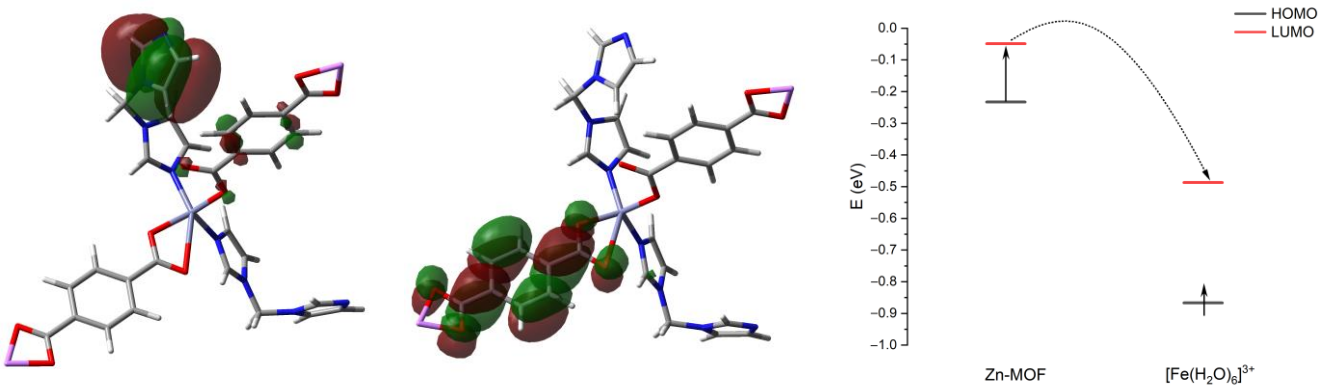

(**a**) (**b**) (**c**)

Figure 6. Results of DFT calculations (B3LYP 6-311 + G(2d,p)) for **Zn-MOF**: (**a**) HOMO isosurface (0.02 a.u.); (**b**) LUMO isosurface (0.02 a.u.); (**c**) Frontier orbital levels of **Zn-MOF** and $[Fe(H_2O)_6]^{3+}$ (restricted open-shell); the PET process is indicated by a curved arrow.

The calculated energy level of **Zn-MOF** LUMO (−0.0486 eV) is higher than the LUMO level of $[Fe(H_2O)_6]^{3+}$ (−0.487 eV); therefore, a photoinduced electron transfer (PET) [42] is possible from the excited state of **Zn-MOF** to Fe^{3+} species (Figure 6), resulting in efficient emission quenching.

3. Materials and Methods

3.1. Synthesis of **Zn-MOF**

Bis(imidazole-1-yl)methane was synthesized analogously to a the procedure reported in [43]. All other materials were obtained from commercial sources and were used as received.

$\{[Zn(bim)(bdc)]\cdot 0.8DMF\cdot 0.4EtOH\cdot 0.1H_2O\}_n$ (Zn-MOF). Bis(imidazol-1-yl)methane (bim) (3.0 mg, 0.02 mmol), terephthalic acid (6.6 mg, 0.04 mmol), and $Zn(NO_3)_2\cdot 6H_2O$ (7.6 mg, 0.02 mmol) were dissolved in DMF/EtOH/H_2O (2:1:1, vol.) mixture (1 mL), placed in a 4 mL screw-cap vial, and heated to 100 °C for 24 h. Colorless block-shaped crystals suitable for SCXRD analysis were separated by filtration with the yield of 7.4 mg (81%). Found, %: C 47.8, H 4.4, N 14.7. $C_{15}H_{12}N_4O_4Zn\cdot 0.8C_3H_7NO\cdot 0.4C_2H_5OH\cdot 0.1H_2O$. Calculated, %: C 47.90, H 4.46, N 14.73. FT-IR: 3439(w), 3124(m), 1674(s), 1600(s), 1504(m), 1392(s), 1352(s), 1226(m), 1143(w), 1089(s), 1018(w), 947(m), 893(w), 842(w), 819(m), 748(s), 709(m), 655(m), 582(m), 513(w).

3.2. Spectral Methods and Elemental Analysis

The IR spectrum for Zn-MOF was recorded in the range of 4000–450 cm^{-1} on Scimitar FTS 2000 Spectrometer (Digilab LLC, Randolph, MA, USA) using KBr pellets. Elemental analysis was carried out using Vario MicroCube CHN(S) analyzer (Elementar Analysensysteme GmbH, Langenselbold, Germany). Thermogravimetric data were obtained by using a NETZSCH TG 209 F1 Iris Thermo Microbalance (Erich NETZSCH GmbH & Co. Holding KG, Selb, Germany) in an argon atmosphere from 30 to 610 °C at a 10 °C/min heating rate. Powder X-ray diffraction (PXRD) analysis was performed on a Bruker D8 ADVANCE diffractometer, equipped with the linear detector LYNXEYE XE-T (Bruker Corporation, Billerica, MA, USA), Cu-Kα radiation, λ = 1.5418 Å. Luminescence spectra were measured by using a HORIBA Fluorolog 3 spectrofluorimeter (HORIBA Jobin Yvon SAS, Edison, NJ, USA), using a 450 W ozone-free xenon lamp as an excitation source and a PC177CE-010 module with R2658 photomultiplier for the detection of the emitted photons.

3.3. X-ray Crystal Structure Determination

The diffraction data of **Zn-MOF** were measured at 290 (2) K on an automated Agilent Xcalibur four-circle diffractometer equipped with an area AtlasS2 detector. Graphite-

monochromated MoKα radiation (λ = 0.71073 Å) was used. Absorption corrections were applied with the use of the SADABS program [44]. The crystal structures were solved and refined by means of the SHELXT [45] and SHELXL [46] programs. Atomic thermal displacement parameters for non-hydrogen atoms except some solvate molecules were refined anisotropically. The positions of hydrogen atoms were calculated corresponding to their geometrical conditions and refined using the riding model. The crystallographic data and details of the structure refinement are summarized in Table 1. Selected geometric parameters of **Zn-MOF** are summarized in Table 2. CCDC 2,264,504 contains the supplementary crystallographic data for this paper. These data can be obtained free of charge from The Cambridge Crystallographic Data Center at http://www.ccdc.cam.ac.uk/data_request/cif (accessed on 21 June 2023).

Table 1. Crystallographic data of **Zn-MOF**.

Parameter	Value
Empirical formula	$C_{15}H_{12}N_4O_4Zn$
Formula weight	377.68
Temperature, K	290 (2)
Crystal system	tetragonal
Space group	*P*42/*n*
a, Å	18.3186 (3)
b, Å	18.3186 (3)
c, Å	11.6298 (4)
Volume, Å^3	3902.62 (19)
Z	8
ρ_{calc}, g/cm^3	1.283
μ, mm^{-1}	1.281
F(000)	1530
Crystal size, mm^3	0.10 × 0.05 × 0.05
2Θ range for data collection, °	4.724 to 57.388
Index ranges	$-18 \leq h \leq 22$ $-18 \leq k \leq 21$ $-15 \leq l \leq 13$
Reflections collected	13026
Independent reflections	4505 (R_{int} = 0.021, R_{sigma} = 0.0239)
Restraints/Parameters	0/267
Goodness-of-fit on F^2	1.047
Final R indexes (I ≥ 2σ (I))	R_1 = 0.0487, wR_2 = 0.0965
Final R indexes (all data)	R_1 = 0.0358, wR_2 = 0.0898
Largest diff. peak/hole, e·Å^{-3}	0.375/−0.320

Table 2. Selected geometric parameters of **Zn-MOF (Å, °)**.

Parameter	Value	Parameter	Value
Zn1—N202	1.941 (15)	Zn1—N2	2.0414 (18)
Zn1—O3	1.9435 (15)	Zn1—C5	2.581 (2)
Zn1—O1	1.9870 (16)		
N202—Zn1—O3	103.9 (4)	N2—Zn1—C5	130.57 (8)
N202—Zn1—O1	110.2 (4)	C5—O1—Zn1	103.41 (16)
O3—Zn1—O1	133.47 (7)	C1—O3—Zn1	118.69 (14)
N202—Zn1—N2	103.0 (3)	C10—N2—Zn1	132.10 (15)
O3—Zn1—N2	98.70 (7)	C12—N2—Zn1	122.28 (16)
O1—Zn1—N2	103.20 (7)	O2—C5—Zn1	74.56 (15)
N202—Zn1—C5	104.3 (3)	O1—C5—Zn1	48.48 (12)
O3—Zn1—C5	113.43 (8)	C2—C5—Zn1	165.7 (2)

3.4. Luminescence Sensing Experiment

To prepare a stable suspension, 23 mg of finely powdered **Zn-MOF** was dispersed into 46 mL of ethanol by sonicating for 30 min. The resulting suspension was left to settle for 1 h, after which a stable suspension (supernatant) was collected and used for the luminescence sensing experiments. For sensing experiments, 2 mL of **Zn-MOF** blank suspension were placed into a quartz cuvette (optical path 1 cm) and the luminescence spectra were recorded after addition of the analyte solution (20 μL of $1 \cdot 10^{-2}$ M solution).

3.5. Computational Chemistry Details

The calculations were performed using Gaussian 09 package [47]. The geometries of Zn-MOF model, $[Li_2Zn(bim)_2(bdc)_2]$ and $[Fe(H_2O)_6]^{3+}$ were optimized using DFT B3LYP [48–51] 6–311 + G(2d,p) [52–55] model chemistry. An empirical dispersion correction was applied using the D3 version of Grimme's empirical dispersion with Becke–Johnson damping [56]. Lack of imaginary vibration modes for the optimized structures indicated their correspondence to minima on the potential energy surfaces. For **Zn-MOF**, all calculations were carried out for a singlet state using the restricted Kohn–Sham approximation, while for $[Fe(H_2O)_6]^{3+}$, a high-spin sextet state (S = 5/2) was considered under unrestricted Kohn–Sham approximation. This state was shown to be the most stable among hexaaquairon(III) species [57].

4. Conclusions

In summary, a new coordination polymer, $\{[Zn(bim)(bdc)]\cdot 0.8DMF\cdot 0.4EtOH\cdot 0.1H_2O\}_n$ (**Zn-MOF)** was prepared by the reaction of zinc nitrate with bis(imidazol-1-yl)methane and terephthalic acid. The structure of **Zn-MOF** consists of polycatenated layers, which form a supramolecular 3D metal–organic framework with closed voids. After removing the solvent molecules included in the voids, **Zn-MOF** demonstrates high thermal stability up to 340 °C, as well as luminescent properties. Inorganic cation and anion detection experiments demonstrated that **Zn-MOF** exhibits a selective luminescence quenching response to Fe^{3+} ions and chromate/dichromate anions. Photoinduced electron transfer from **Zn-MOF** to Fe^{3+} was elucidated as a possible quenching mechanism on the basis of DFT calculations.

Supplementary Materials: The following supporting information can be downloaded at: https://www.mdpi.com/article/10.3390/inorganics11070264/s1, Figure S1: Thermogravimetric plot for **Zn-MOF**; Figure S2: FT-IR spectrum of **Zn-MOF**; Figure S3: Two disordered positions of bim ligand in the structure of **Zn-MOF**; Figure S4: Crystal packing representation (3 × 3 × 3 unit cells) of **Zn-MOF** showing isolated voids; Figure S5: Fingerprint plots from Hirshfeld surface analysis of the crystal structure of **Zn-MOF**; Figure S6: Luminescence excitation and emission spectra of H_2bdc ligand in the solid state; Figure S7: Luminescence excitation and emission spectra of bim ligand in the solid state; Figure S8: Luminescence decay kinetics **Zn-MOF**; Figure S9: Luminescence emission intensity of **Zn-MOF** versus time plot; Figure S10: Luminescence emission spectra of **Zn-MOF** ethanol suspensions in the presence of metal cations; Figure S11: DFT B3LYP 6-311+G(2d,p) optimized structures of **Zn-MOF** model and $[Fe(H_2O)_6]^{3+}$.

Author Contributions: Conceptualization, A.S.P. and V.P.F.; methodology, A.S.P.; investigation, V.V.M., D.I.P. and A.A.R.; writing—original draft preparation, V.V.M.; writing—review and editing, A.S.P.; visualization, D.I.P.; supervision, A.S.P. and V.P.F. All authors have read and agreed to the published version of the manuscript.

Funding: This work was supported by the Ministry of Science and Higher Education of the Russian Federation (Agreement No. 075-15-2022-263). The experiments were performed using large-scale research facilities "EXAFS Spectroscopy Beamline".

Data Availability Statement: The data presented in this study are available on request from the corresponding author.

Acknowledgments: The Siberian Branch of the Russian Academy of Sciences (SB RAS) Siberian Supercomputer Center is gratefully acknowledged for providing supercomputer facilities.

Conflicts of Interest: The authors declare no conflict of interest. The funders had no role in the design of the study; in the collection, analyses, or interpretation of data; in the writing of the manuscript, or in the decision to publish the results.

References

1. Wagner, M.; Andrew Lin, K.-Y.; Oh, W.-D.; Lisak, G. Metal-Organic Frameworks for Pesticidal Persistent Organic Pollutants Detection and Adsorption—A Mini Review. *J. Hazard. Mater.* **2021**, *413*, 125325. [CrossRef]
2. da Costa Filho, B.M.; Duarte, A.C.; Rocha-Santos, T.A.P. Environmental Monitoring Approaches for the Detection of Organic Contaminants in Marine Environments: A Critical Review. *Trends Environ. Anal. Chem.* **2022**, *33*, e00154. [CrossRef]
3. Sousa, J.C.G.; Ribeiro, A.R.; Barbosa, M.O.; Pereira, M.F.R.; Silva, A.M.T. A Review on Environmental Monitoring of Water Organic Pollutants Identified by EU Guidelines. *J. Hazard. Mater.* **2018**, *344*, 146–162. [CrossRef] [PubMed]
4. Han, M.A.; Kim, J.H.; Song, H.S. Persistent Organic Pollutants, Pesticides, and the Risk of Thyroid Cancer: Systematic Review and Meta-Analysis. *Eur. J. Cancer Prev.* **2019**, *28*, 344–349. [CrossRef]
5. Iqubal, A.; Ahmed, M.; Ahmad, S.; Sahoo, C.R.; Iqubal, M.K.; Haque, S.E. Environmental Neurotoxic Pollutants: Review. *Environ. Sci. Pollut. Res.* **2020**, *27*, 41175–41198. [CrossRef]
6. Fuller, R.; Landrigan, P.J.; Balakrishnan, K.; Bathan, G.; Bose-O'Reilly, S.; Brauer, M.; Caravanos, J.; Chiles, T.; Cohen, A.; Corra, L.; et al. Pollution and Health: A Progress Update. *Lancet Planet Health* **2022**, *6*, e535–e547. [CrossRef] [PubMed]
7. Conway, D.; Henderson, M.A. Iron Metabolism. *Anaesth. Intensive Care Med.* **2019**, *20*, 175–177. [CrossRef]
8. Panda, S.K.; Mishra, S.; Singh, A.K. Recent Progress in the Development of MOF-Based Optical Sensors for Fe^{3+}. *Dalton Trans.* **2021**, *50*, 7139–7155. [CrossRef]
9. Guan, B.-B.; Li, Q.; Xu, Y.-T.; Chen, L.-H.; Wu, Z.; Fan, Z.-L.; Zhu, W. Highly Selective and Sensitive Detection towards Cationic Cu^{2+} and Fe^{3+} Contaminants via an In-MOF Based Dual-Responsive Fluorescence Probe. *Inorg. Chem. Commun.* **2020**, *122*, 108273. [CrossRef]
10. Han, L.-J.; Kong, Y.-J.; Xu, Y.-Y.; Huang, M.-M. A Zn-Based Coordination Compound for Fluorescence Detection of Fe^{3+}, Cu^{2+}, Ni^{2+} and CrO_4^{2-} Ions. *Polyhedron* **2021**, *193*, 114868. [CrossRef]
11. Gao, E.; Zhu, M.; Zhang, Y.; Kosinova, M.; Fedin, V.P.; Wu, S. Logic Operation for Differentiation and Speciation of Fe^{3+} and Fe^{2+} Based on Two-Dimensional Metal–Organic Frameworks with Tunable Emissions. *Appl. Organomet. Chem.* **2021**, *35*, e6129. [CrossRef]
12. Huang, L.; Ran, Z.; Liu, X.; Huang, C.-M.; Qin, Q.-P.; Zhou, J. One Luminescent Cadmium Iodide with Free Bifunctional Azole Sites as a Triple Sensor for Cu^{2+}, Fe^{3+}, and $Cr_2O_7^{2-}$ Ions. *Inorg. Chem.* **2022**, *61*, 14156–14163. [CrossRef] [PubMed]
13. Wang, F.; Zhang, F.; Zhao, Z.; Sun, Z.; Pu, Y.; Wang, Y.; Wang, X. Multifunctional MOF-Based Probes for Efficient Detection and Discrimination of Pb^{2+}, Fe^{3+} and $Cr_2O_7^{2-}/CrO_4^{2-}$. *Dalton Trans.* **2021**, *50*, 12197–12207. [CrossRef]
14. Gao, E.; Liu, D.; Xing, J.; Feng, Y.; Su, J.; Liu, J.; Zhao, H.; Wang, N.; Jia, Z.; Zhang, X.; et al. A Recyclable Bi-Functional Luminescent Zinc (II) Metal–Organic Framework as Highly Selective and Sensitive Sensing Probe for Nitroaromatic Explosives and Fe^{3+} Ions. *Appl. Organomet. Chem.* **2019**, *33*, e5109. [CrossRef]
15. Yu, X.; Ryadun, A.A.; Kovalenko, K.A.; Guselnikova, T.; Ponomareva, V.G.; Potapov, A.; Fedin, V.P. 4 in 1: Multifunctional Europium-Organic Framework with Luminescent Sensing Properties, White Light Emission, Proton Conductivity and Reverse Acetylene-Carbon Dioxide Adsorption Selectivity. *Dalton Trans.* **2023**. [CrossRef]
16. Liu, J.-Q.; Luo, Z.-D.; Pan, Y.; Kumar Singh, A.; Trivedi, M.; Kumar, A. Recent Developments in Luminescent Coordination Polymers: Designing Strategies, Sensing Application and Theoretical Evidences. *Coord. Chem. Rev.* **2020**, *406*, 213145. [CrossRef]
17. Gorai, T.; Schmitt, W.; Gunnlaugsson, T. Highlights of the Development and Application of Luminescent Lanthanide Based Coordination Polymers, MOFs and Functional Nanomaterials. *Dalton Trans.* **2021**, *50*, 770–784. [CrossRef] [PubMed]
18. Ma, Y.; Zhu, M.; Zhang, Y.; Sun, Y.; Wu, S. A Water-Stable Eu-MOF as Multi-Responsive Luminescent Sensor for High-Efficiency Detection of Fe^{3+}, MnO_4^- Ions and Nicosulfuron in Aqueous Solution. *J. Solid State Chem.* **2022**, *316*, 123598. [CrossRef]
19. Parmar, B.; Bisht, K.K.; Rachuri, Y.; Suresh, E. Zn(Ii)/Cd(Ii) Based Mixed Ligand Coordination Polymers as Fluorosensors for Aqueous Phase Detection of Hazardous Pollutants. *Inorg. Chem. Front.* **2020**, *7*, 1082–1107. [CrossRef]
20. Kuznetsova, A.; Matveevskaya, V.; Pavlov, D.; Yakunenkov, A.; Potapov, A. Coordination Polymers Based on Highly Emissive Ligands: Synthesis and Functional Properties. *Materials* **2020**, *13*, 2699. [CrossRef]
21. Pfaffeneder, T.; Bauer, W.; Weber, B. X-ray Structure and Magnetic Properties of Two New Iron(II) 1D Coordination Polymers with Bis(Imidazolyle)Methane as Bridging Ligand. *Z. Anorg. Allg. Chem.* **2010**, *636*, 183–187. [CrossRef]
22. Barsukova, M.; Goncharova, T.; Samsonenko, D.; Dybtsev, D.; Potapov, A. Synthesis, Crystal Structure, and Luminescent Properties of New Zinc(II) and Cadmium(II) Metal-Organic Frameworks Based on Flexible Bis(Imidazol-1-yl)Alkane Ligands. *Crystals* **2016**, *6*, 132. [CrossRef]
23. Barsukova, M.O.; Sapchenko, S.A.; Kovalenko, K.A.; Samsonenko, D.G.; Potapov, A.S.; Dybtsev, D.N.; Fedin, V.P. Exploring the Multifunctionality in Metal-Organic Framework Materials: How Do the Stilbenedicarboxylate and Imidazolyl Ligands Tune the Characteristics of Coordination Polymers? *New J. Chem.* **2018**, *42*, 6408–6415. [CrossRef]
24. Du, Z.-Y.; Xue, Y.-N.; Liu, X.-M.; Li, N.-F.; Wang, J.-L.; Mei, H.; Xu, Y. An unprecedented polyoxometalate-encapsulated organo–metallophosphate framework as a highly efficient cocatalyst for CO_2 photoreduction. *J. Mater. Chem. A* **2022**, *10*, 3469–3477. [CrossRef]

25. Zhang, X.-F.; Song, W.-C.; Yang, Q.; Bu, X.-H. Zn(II) and Cd(II) Coordination Polymers Assembled by Di(1H-Imidazol-1-Yl)Methane and Carboxylic Acid Ligands. *Dalton Trans.* **2012**, *41*, 4217–4223. [CrossRef] [PubMed]
26. Jin, S.; Wang, D.; Chen, W. Synthesis, Luminescence, and Structural Characterization of Zn and Cd Coordination Polymers of Flexible Bis(Imidazolyl) Derivatives. *Inorg. Chem. Commun.* **2007**, *10*, 685–689. [CrossRef]
27. Zhang, T.; Zhao, Y.J.; Qin, Q.P. Two N-Donor Auxiliary Ligands Mediated Zn(II) Coordination Polymers Incorporating 5-Nitro-1,2,3-Benzenetricarboxylate Ligand: Syntheses, Crystal Structures, and Luminescent Properties. *Jiegou Huaxue* **2020**, *39*, 1051–1056. [CrossRef]
28. Zhao, J.; Dong, W.W.; Li, C.; Mou, Y.Q.; Mu, Z.H.; Li, D.S. Encapsulation of Discrete $(H_2O)_4$ Clusters in a 1D Tube-Like Metal-Organic Coordination Polymer. *Synth. React. Inorg. Met. Org. Nano-Met. Chem.* **2012**, *42*, 628–633. [CrossRef]
29. Jin, S.; Wang, D.; Xu, Y. Five New Metal(II) Complexes with 3-D Network Structures Based on Carboxylate and Bis(Imidazole) Ligands: Syntheses and Structures. *J. Coord. Chem.* **2012**, *65*, 1953–1969. [CrossRef]
30. Dinda, S.; Pahari, G.; Maiti, A.; Ghoshal, D. Solvent Induced Reversible Single-Crystal-to-Single-Crystal Structural Transformation in Dynamic Metal Organic Frameworks: A Case of Enhanced Hydrogen Sorption in Polycatenated Framework. *CrystEngComm* **2023**, *25*, 1116–1125. [CrossRef]
31. Schuitema, A.M.; Engelen, M.; Koval, I.A.; Gorter, S.; Driessen, W.L.; Reedijk, J. New Didentate Bispyrazole Ligands Forming Uncommon Eight-Ring Chelates with Divalent Copper, Zinc and Cobalt. *Inorg. Chim. Acta* **2001**, *324*, 57–64. [CrossRef]
32. Deacon, G.B.; Phillips, R.J. Relationships between the Carbon-Oxygen Stretching Frequencies of Carboxylato Complexes and the Type of Carboxylate Coordination. *Coord. Chem. Rev.* **1980**, *33*, 227–250. [CrossRef]
33. Addison, A.W.; Rao, T.N.; Reedijk, J.; van Rijn, J.; Verschoor, G.C. Synthesis, Structure, and Spectroscopic Properties of Copper(II) Compounds Containing Nitrogen-Sulphur Donor Ligands; the Crystal and Molecular Structure of Aqua[1,7-Bis(N-Methylbenzimidazol-2′-yl)-2,6-Dithiaheptane]Copper(II) Perchlorate. *J. Chem. Soc. Dalton Trans.* **1984**, *7*, 1349–1356. [CrossRef]
34. Tian, J.-L.; Cui, G.-H.; Batten, S.R.; Li, J.-R.; Bu, X.-H. Multidimensional Metal−Organic Frameworks Constructed from Flexible Bis(Imidazole) Ligands. *Cryst. Growth. Des.* **2005**, *5*, 1775–1780. [CrossRef]
35. Masciocchi, N.; Pettinari, C.; Alberti, E.; Pettinari, R.; Di Nicola, C.; Figini Albisetti, A.; Sironi, A. Structural and Thermodiffractometric Analysis of Coordination Polymers. Part II:1 Zinc and Cadmium Derivatives of the Bim Ligand [Bim = Bis(1-Imidazolyl)Methane]. *Inorg. Chem.* **2007**, *46*, 10501–10509. [CrossRef] [PubMed]
36. Blatov, V.A.; Shevchenko, A.P.; Proserpio, D.M. Applied Topological Analysis of Crystal Structures with the Program Package ToposPro. *Cryst. Growth. Des.* **2014**, *14*, 3576–3586. [CrossRef]
37. Spackman, P.R.; Turner, M.J.; McKinnon, J.J.; Wolff, S.K.; Grimwood, D.J.; Jayatilaka, D.; Spackman, M.A. CrystalExplorer: A Program for Hirshfeld Surface Analysis, Visualization and Quantitative Analysis of Molecular Crystals. *J. Appl. Cryst.* **2021**, *54*, 1006–1011. [CrossRef] [PubMed]
38. Burlak, P.V.; Kovalenko, K.A.; Samsonenko, D.G.; Fedin, V.P. Cadmium(II)-Organic Frameworks Containing the 1,3-Bis(2-Methylimidazolyl)Propane Ligand. *Russ. J. Coord. Chem.* **2022**, *48*, 504–509. [CrossRef]
39. Burlak, P.V.; Samsonenko, D.G.; Kovalenko, K.A.; Fedin, V.P. Synthesis, Structure and Luminescent Properties of Zn(II) Metal–Organic Frameworks Constructed by Flexible and Rigid Ligands. *Polyhedron* **2022**, *222*, 115880. [CrossRef]
40. Yu, X.; Ryadun, A.A.; Potapov, A.S.; Fedin, V.P. Ultra-Low Limit of Luminescent Detection of Gossypol by Terbium(III)-Based Metal-Organic Framework. *J. Hazard. Mater.* **2023**, *452*, 131289. [CrossRef]
41. Pavlov, D.I.; Sukhikh, T.S.; Ryadun, A.A.; Matveevskaya, V.V.; Kovalenko, K.A.; Benassi, E.; Fedin, V.P.; Potapov, A.S. A Luminescent 2,1,3-Benzoxadiazole-Decorated Zirconium-Organic Framework as an Exceptionally Sensitive Turn-On Sensor for Ammonia and Aliphatic Amines in Water. *J. Mater. Chem. C Mater.* **2022**, *10*, 5567–5575. [CrossRef]
42. Haldar, R.; Ghosh, A.; Maji, T.K. Charge Transfer in Metal–Organic Frameworks. *Chem. Commun.* **2023**, *59*, 1569–1588. [CrossRef]
43. Barsukova, M.O.; Samsonenko, D.G.; Goncharova, T.V.; Potapov, A.S.; Sapchenko, S.A.; Dybtsev, D.N.; Fedin, V.P. Coordination Polymers with Adjustable Dimensionality Based on CuII and Bis-Imidazolyl Bridging Ligand. *Russ. Chem. Bull.* **2016**, *65*, 2914–2919. [CrossRef]
44. Sheldrick, G.M. *SADABS, Program for Empirical X-ray Absorption Correction*; ScienceOpen, Inc.: Burlington, MA, USA, 1996.
45. Sheldrick, G.M. SHELXT—Integrated Space-Group and Crystal-Structure Determination. *Acta Crystallogr. Sect. A* **2015**, *71*, 3–8. [CrossRef]
46. Sheldrick, G.M. Crystal Structure Refinement with SHELXL. *Acta Crystallogr. Sect. C* **2015**, *71*, 3–8. [CrossRef]
47. Frisch, M.J.; Trucks, G.W.; Schlegel, H.B.; Scuseria, G.E.; Robb, M.A.; Cheeseman, J.R.; Scalmani, G.; Barone, V.; Mennucci, B.; Petersson, G.A.; et al. *Gaussian 09, Rev. D.01*; Gaussian, Inc.: Wallingford, CT, USA, 2013.
48. Becke, A.D. Density-Functional Exchange-Energy Approximation with Correct Asymptotic Behavior. *Phys. Rev. A* **1988**, *38*, 3098–3100. [CrossRef] [PubMed]
49. Lee, C.; Yang, W.; Parr, R.G. Development of the Colle-Salvetti Correlation-Energy Formula into a Functional of the Electron Density. *Phys. Rev. B* **1988**, *37*, 785–789. [CrossRef] [PubMed]
50. Vosko, S.H.; Wilk, L.; Nusair, M. Accurate Spin-Dependent Electron Liquid Correlation Energies for Local Spin Density Calculations: A Critical Analysis. *Can. J. Phys.* **1980**, *58*, 1200–1211. [CrossRef]
51. Stephens, P.J.; Devlin, F.J.; Chabalowski, C.F.; Frisch, M.J. Ab Initio Calculation of Vibrational Absorption and Circular Dichroism Spectra Using Density Functional Force Fields. *J. Phys. Chem.* **1994**, *98*, 11623–11627. [CrossRef]

52. McLean, A.D.; Chandler, G.S. Contracted Gaussian Basis Sets for Molecular Calculations. I. Second Row Atoms, $Z = 11 - 18$. *J. Chem. Phys.* **1980**, *72*, 5639–5648. [CrossRef]
53. Krishnan, R.; Binkley, J.S.; Seeger, R.; Pople, J.A. Self-consistent Molecular Orbital Methods. XX. A Basis Set for Correlated Wave Functions. *J. Chem. Phys.* **1980**, *72*, 650–654. [CrossRef]
54. Clark, T.; Chandrasekhar, J.; Spitznagel, G.W.; Schleyer, P.V.R. Efficient Diffuse Function-augmented Basis Sets for Anion Calculations. III. The 3-21+G Basis Set for First-row Elements, Li–F. *J. Comput. Chem.* **1983**, *4*, 294–301. [CrossRef]
55. Frisch, M.J.; Pople, J.A.; Binkley, J.S. Self-consistent Molecular Orbital Methods 25. Supplementary Functions for Gaussian Basis Sets. *J. Chem. Phys.* **1984**, *80*, 3265–3269. [CrossRef]
56. Grimme, S.; Ehrlich, S.; Goerigk, L. Effect of the Damping Function in Dispersion Corrected Density Functional Theory. *J. Comput. Chem.* **2011**, *32*, 1456–1465. [CrossRef]
57. Harris, D.; Loew, G.H.; Komornicki, A. Structure and Relative Spin-State Energetics of $[Fe(H_2O)_6]^{3+}$: A Comparison of UHF, Møller–Plesset, Nonlocal DFT, and Semiempircal INDO/S Calculations. *J. Phys. Chem. A* **1997**, *101*, 3959–3965. [CrossRef]